Shear-Induced Mixing Governs Codeformation of Crystalline-Amorphous Nanolaminates

Wei Guo,[1,*] Eric A. Jägle,[1] Pyuck-Pa Choi,[1] Jiahao Yao,[2] Aleksander Kostka,[1] Jochen M. Schneider,[3] and Dierk Raabe[1,†]

[1]*Max Planck Institut für Eisenforschung, Düsseldorf 40237, Germany*
[2]*Shenyang National Laboratory for Materials Science, Institute of Metal Research, Chinese Academy of Sciences,*
Shenyang 110016, China
[3]*Materials Chemistry, RWTH Aachen University, Kopernikusstr. 10, D-52074 Aachen, Germany*

Deformation of ductile crystalline-amorphous nanolaminates is not well understood due to the complex interplay of interface mechanics, shear banding, and deformation-driven chemical mixing. Here we present indentation experiments on 10 nm nanocrystalline Cu–100 nm amorphous CuZr model multilayers to study these mechanisms down to the atomic scale. By using correlative atom probe tomography and transmission electron microscopy we find that crystallographic slip bands in the Cu layers coincide with noncrystallographic shear bands in the amorphous CuZr layers. Dislocations from the crystalline layers drag Cu atoms across the interface into the CuZr layers. Also, crystalline Cu blocks are sheared into the CuZr layers. In these sheared and thus Cu enriched zones the initially amorphous CuZr layer is rendered into an amorphous plus crystalline nanocomposite.

Metallic crystalline-amorphous nanolaminate composites have been reported to be both ductile and strong [1–8]. The reason for this mechanical response is not understood since glassy compounds usually fail already at low strains [9–11].

For identifying the codeformation mechanisms in such composites, we synthesized and indented model nanolaminates consisting of nanocrystalline Cu and amorphous $Cu_{54}Zr_{46}$. The alternating layers were deposited on Si (100) wafers by magnetron sputtering using pure Cu and Zr targets (99.99 at. %) [12]. The base pressure was below 4×10^{-5} Pa and the processing pressure was 4×10^{-1} Pa Ar. The thickness of the crystalline Cu and amorphous CuZr layers was 10 and 100 nm, respectively. The total thickness of the Cu/CuZr multilayer stack with a cap CuZr layer on the top was ∼1200 nm. The Cu nanocrystals had a ⟨111⟩ fiber texture, measured by XRD. The nanolaminates were indented with a 10 g Vickers indenter for 10 s [Fig. 1(a)].

To study nanostructural and atomic-scale chemical deformation effects at the same position we performed a joint analysis by transmission electron microscopy (TEM) and atom probe tomography (APT) [13–15]. TEM lamellae of ≈100 nm thickness were prepared by an *in situ* lift-out method and focused-ion-beam (FIB) milling. A 200 kV Jeol JEM-2200FS TEM was used for high-resolution TEM and nanobeam diffraction (NBD). For the correlative TEM-APT analysis, tip-shaped specimens containing deformation shear bands were cut by site-specific preparation, mounted onto an electropolished bisected TEM Cu grid, and thinned by annular FIB milling. APT was performed with a local electrode atom probe (LEAP 3000X HR). Samples were analyzed at 60 K, applying 532 nm

wavelength 10 ps laser pulses of 0.4 nJ with a repetition rate of 250 kHz. The data sets were reconstructed using the software IVAS 3.6.6 (CAMECA Instruments) [16,17].

APT analyses of as-deposited samples were performed with the tip evaporation direction both perpendicular and parallel to the CuZr/Cu interfaces. The Cu concentration is 54.2 ± 0.3 at. % in the amorphous CuZr layers and 99.2 ± 0.5 at. % in the Cu layers. The laminates contain traces of impurity oxygen from sputtering [18]. The width of interfaces oriented perpendicular to the analysis direction is ∼1.5 nm for the CuZr/Cu interfaces and ∼4 nm for the Cu/CuZr interfaces. This difference is due to ion trajectory aberrations at the interface when the tip is evaporated from the CuZr layer with a lower field of evaporation to the Cu layer with a higher field of evaporation, resulting in an apparent interfacial width compression, and, vice versa, to an apparent interfacial width expansion for the opposite layer evaporation sequence. From measurements with the interfaces parallel to the evaporation direction, the interfaces were found to be more symmetric with a width of ∼3 nm. This high value is due to local magnification [19] and interface roughness.

After indentation, sharp shear bands around the pileup regions are observed, Figs. 1(a)–1(c). The Cu layers are not significantly reduced in thickness in most pileup regions. However, they are deformed to a thickness of ∼2.5 nm inside the shear bands. Figures 1(d)–1(e) show the correlative TEM and APT analysis. The area in the bright field TEM micrograph of an APT specimen highlighted in yellow is the volume containing a shear band analyzed by APT, Fig. 1(d). The yellow lines mark a region representing the volume investigated by APT although the actual APT data in Fig. 1(e) were taken from a slightly
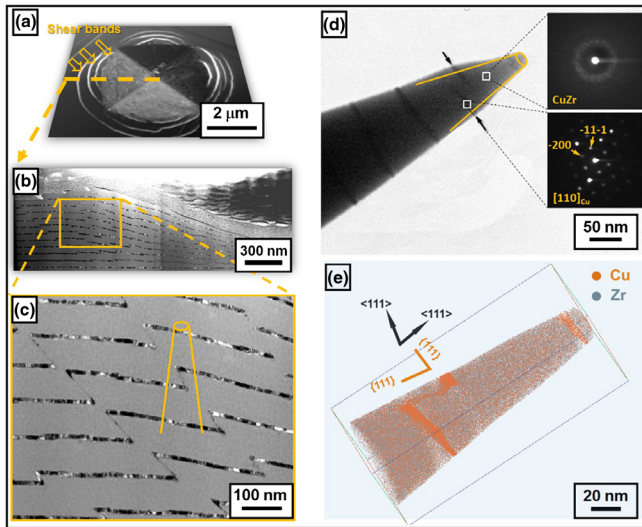
FIG. 1 (color online). (a) SEM view of CuZr/Cu multilayers after Vickers indentation with a load of 10 g. (b) Cross-sectional view of shear bands beneath an indent. (c) Bright field TEM image of an area containing shear bands. The yellow lines mark a region investigated by APT [the data in (e) were taken from a slightly different region in the same sample). (d) Bright field TEM image of an APT tip with corresponding CuZr and Cu nanobeam diffraction patterns. The arrows point to the shear band region. The TEM image of the APT tip provides crystallographic information of the sheared Cu layer. (e) APT reconstructed volume from the exact APT tip shown in (d).
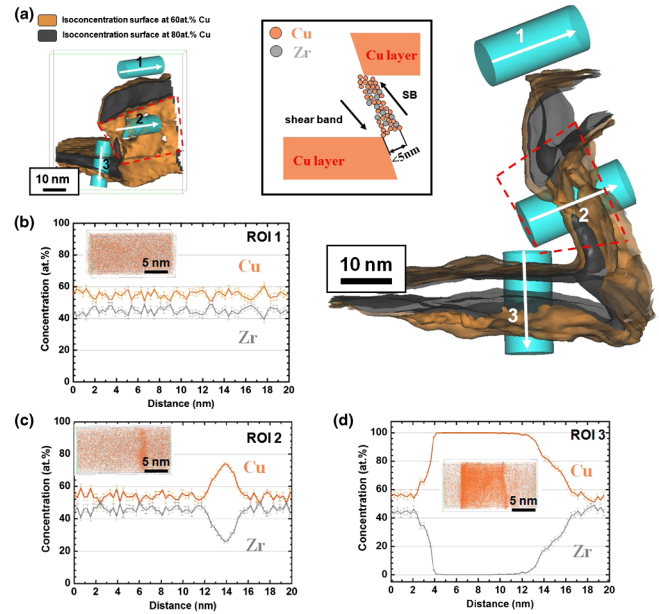

FIG. 2 (color online). (a) Two different 3D Cu isoconcentration surface views and a schematic of a portion of the same APT measurement presented in Fig. 1 containing a shear band. Also shown are several regions of interest (ROIs) above and within the shear band (ROI 1 and ROI 2) and outside of the shear band (ROI 3), which are selected for further chemical analysis; their 1D-concentration profiles are shown in (b), (c), and (d), respectively.

different region in the same sample. The white rectangles in Fig. 1(d) indicate regions from which NBD patterns were acquired. They show crystalline diffraction spots in the Cu region and an amorphous halo in the CuZr region. Figure 1(e) reveals the atomic composition of the sheared region taken by APT together with the crystallographic orientation obtained from TEM. It shows that the {111} planes of the Cu are parallel to the interface plane of the shear band.

Figures 1(c)–1(e) reveal zones with a large and very sharp, abruptly sheared Cu layer offset> 30 nm. The layer is not completely disconnected from the sheared region though. Instead, it is heavily deformed at a 70.5° tilt angle to the interface plane, which corresponds to the {111} planes in Cu. In the shear band region, the Cu layers are subjected to a huge true shear strain of 4.0 ± 0.2, as calculated from the layer displacement. The observations indicate dislocation slip on {111} planes in the Cu. The large displacement (> 30 nm) of the sheared and fragmented Cu layer shown in Fig. 1(e) suggests that large numbers of Cu dislocations accommodate the shear inside the crystalline phase, extending it across the Cu/CuZr interface into the initially amorphous layer.

The 60 at. % isoconcentration Cu surface [Fig. 2(a)] indicates that chemical mixing between the crystalline and amorphous phase has occurred along the shear offset of the Cu layer. Several regions in this zone were probed for

composition [Figs. 2(b)–2(d)]. A nonsheared amorphous region is shown for reference in Fig. 2(b). Although this amorphous region was also near the shear band zone it does not indicate any remarkable chemical fluctuations compared to the as-deposited amorphous CuZr layer (Cu 55.1 ± 2.1 at. %, Zr44.9 ± 2.1 at. % in average). In contrast, the concentrations mapped across the shear band that penetrated both the Cu layer and the amorphous zone below it [Fig. 2(c)] show strong Cu enrichment (∼68 at. % in average) of ∼2.5 nm thickness in the sheared portion of the CuZr layer. The concentration and the interfacial width of the remaining Cu layer does not change [Fig. 2(d)] compared to the as-deposited state. This indicates that deformation-induced mixing occurs only within a narrow region (∼2.5 nm) inside the shear band [20,21].

The sampling region marked by red lines in Fig. 2(a) (size: $9 \times 32 \times 32$ nm^3) represents the mixing zone inside the shear band, where Cu atoms have been displaced out of the crystalline Cu layer and into the initially amorphous CuZr region. We use the position of the original Cu layer as coordinate origin and the longitudinal axis corresponds to the dislocation slip direction inside the crystalline Cu. Along the shear direction, the chemical concentration of Cu varies from 60 to 88 at. %, where the average number of atoms in each sampling bin (0.3 nm width) is ∼3000. The mean displacement of the Cu atoms in this shear region is calculated by $\lambda = [\sum_{i=1}^{N} (C_i - C_1)n_i d_i]/ [\sum_{i=1}^{N} (C_i - C_1)n_i]$, where C_i is the Cu concentration in

TABLE I. Chemical analysis of different regions as measured by APT.

	Cu layer thickness (nm)	Interface width (nm)	Max. Cu (at. %)	Aver. Cu (at. %)	Max. Zr (at. %)	Aver. Zr (at. %)
Cu layer as deposited	~10	~2.5	99.9 ± 0.1	99.7 ± 0.3	0.1 ± 0.1	0.3 ± 0.3
Cu enriched region inside shear band	2.5	< 1.5	73.0 ± 2.8	64.9 ± 2.3	27.1 ± 2.8	35.2 ± 2.3
	3	< 1.5	69.0 ± 2.5	64.6 ± 3.7	31.0 ± 2.4	35.4 ± 3.4
	2.5	< 1.5	95.4 ± 0.7	86.5 ± 1.7	4.6 ± 0.6	13.5 ± 1.6
	2	< 1.5	72.8 ± 2.9	67.3 ± 3.0	27.2 ± 2.8	22.7 ± 3.0
Cu layer outsideshear band	~8	~2.5	99.8 ± 0.2	99.2 ± 0.4	0.2 ± 0.1	0.8 ± 0.4
	~10	~2.5	99.8 ± 0.2	99.4 ± 0.3	0.2 ± 0.1	0.6 ± 0.3
Shear band region above the Cu shear offset			56.0 ± 2.1	54.4 ± 2.0	44.0 ± 2.0	45.6 ± 2.0

one sampling bin $(9 \times 32 \times 0.3 \text{ nm}^3)$, C_1 is the Cu concentration in the CuZr layer in the as-deposited state, n_i is the number of atoms in the ith bin, and d_i is the distance between the ith bin and the original Cu layer position. $(C_i - C_1)n_i$ is the number of displaced Cu atoms inside the ith bin. This estimate gives a mean shear displacement of the Cu atoms stemming from the crystalline layer of 11.75 ± 1.50 nm into the amorphous CuZr region. For the time elapsed during this displacement we use the indentation time $(t = 10 \text{ s})$ as an upper bound, knowing that shear band events occur more abruptly. The associated pseudo diffusion coefficient is $D = \lambda^2/4t \approx 2.30 \times 10^{-14} \text{ cm}^2/\text{s}$, which is 24 orders of magnitude above Cu self-diffusion at room temperature [22]. We use Cu self-diffusion as an approximation as no literature is available about the diffusion coefficient of Cu in amorphous CuZr.

To understand the observed deformation-induced atomic mixing, we probe several compositional profiles across the Cu enriched region inside the shear band. Several regions across the Cu layer and outside the shear band were also analyzed (Table I) for reference. The interface width here is defined as the average spacing of the two interfaces pertaining to one Cu layer. This analysis reveals that mixing in the sheared regions of the Cu layer is caused by the shear band running through it: in this mixing zone the Cu concentration varies from 64.6 to 95.4 at. % within a narrow shear layer thickness range of only 2–3 nm. In contrast, no excess Cu is found above that shear band; i.e., mixing is confined to a very narrow zone. The accelerated transport of Cu from the Cu layer into the CuZr region (see the estimate of the diffusion coefficient) occurs only inside the shear band. Regions outside the shear band have the same interface width and concentration profiles as the as-deposited layers; i.e., they do not undergo deformation-driven mixing.

Figure 3 shows high-resolution TEM (HRTEM) images obtained from the sheared offset region of shear bands in the 100 nm CuZr–10 nm Cu multilayer specimen. Attention is placed on the mixing inside the initially amorphous CuZr zone, caused by atoms that are sheared out of the Cu layer into the metallic glass. Several spots

along the shear band were selected for structural analysis. Figure 3(b) shows a HRTEM image and NBD patterns along the pathway of a shear band (spots 2–7) and, as reference, from a region inside the undeformed amorphous layer (spot 1). The sizes of the circles indicate the diameter of the diffraction aperture. NBD at spot 1 shows no crystalline diffraction but only a halo typical of an
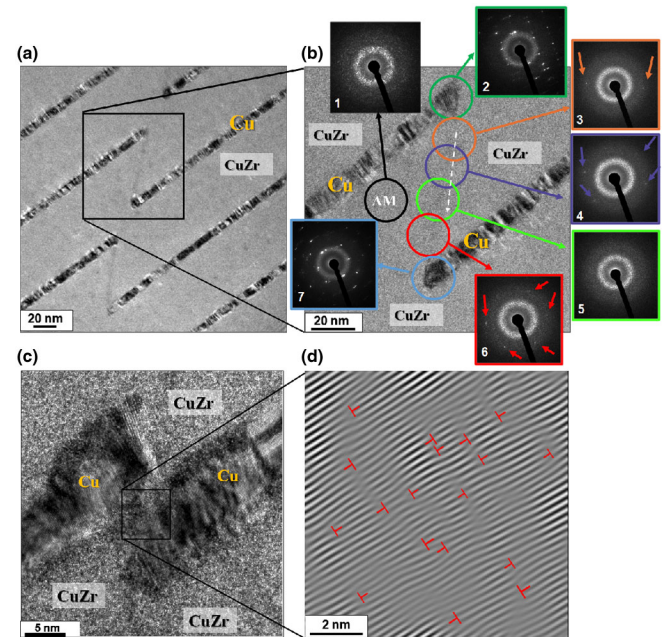

FIG. 3 (color online). HRTEM observations of shear bands in 100 nm CuZr–10 nm Cu multilayers subjected to different shear strains. (a) HRTEM image of an area containing several cross-phase shear bands with high shear strain. (b) HRTEM image together with NBD patterns along the pathway of a selected shear band (spots 2–7) and from a region in the amorphous layer (spot 1). The sizes of the circles indicate the diameter of the diffraction aperture. Some of the NBD patterns show both an inner halo ring (amorphous) and some weak discrete diffraction spots (crystalline) outside of the inner halo ring (see small arrows, NBD spots 3,4,6). (c) HRTEM image of the area containing a shear band with a shear strain ~1.0. (d) Inverse FFT image using only the {111} reflections in the strain localized region indicated in (c).

amorphous structure. NBD spots 2 and 7 are given as references for dominantly crystalline material associated to nonsheared portions of the Cu layers close to the shear band.

Surprisingly, some of the NBD patterns taken along the shear band penetrating the initially amorphous CuZr layer show both an inner halo ring (amorphous material) as well as some weak discrete diffraction spots (crystalline material) outside of the inner halo ring (arrows, NBD spots 3,4,6). This means that the initially amorphous CuZr layer has been rendered into an amorphous plus crystalline composite by the shear band and the associated mixing as proven by the diffraction spots 3, 4, and 6.

This indicates that the crystalline diffraction spots stem either from jointly sheared Cu fragments of the crystalline layer or from a portion inside the initially amorphous regions that crystallized due to the increase in Cu content. The lattice parameter of $d_{(111)} = 0.209$ nm, determined from FFT diffraction patterns, supports the possibility that compact nanocrystalline Cu portions might have been displaced by the shear band into the initially amorphous CuZr zone.

The absence of clearly visible crystalline diffraction spots in the NBD pattern taken at spot 5 suggests that this region remained amorphous. Figures 3(c) and 3(d) show a similar shear region. Here a clearly crystalline structure containing a very high dislocation content can be observed inside the initially amorphous CuZr zone.

A number of very similarly sheared and, hence, mixed regions have been observed and characterized as demonstrated in the attached Supplemental Material [23]. Figures SM1(a)–SM1(c) show three APT data sets obtained from the 100 nm CuZr–10 nm Cu multilayer system after indentation with a 10 g load at various strains [23]. The local strains were obtained by quantifying the offset among neighboring layers. One-dimensional-Cu concentration profiles taken perpendicular through the shear banded regions inside the originally amorphous layers are shown in Fig. SM1(d) and marked by arrows [23].

Following a similar motivation several related studies on deformation-driven mixing were conducted in the field of severe plastic deformation using electron microscopy and APT [20,21], [24–29]. In these works several types of crystalline systems, often with small mutual solubility, were exposed to very large strains via ball milling, high pressure torsion, or wire drawing. The difference is that here we study codeformation of a crystal or metallic glass nanocomposite and consider the mixing mechanisms associated with the early stages of the deformation process rather than after severe deformation. Also, the shear banded regions are here probed using correlative TEM-APT methods [14].

In Fig. 4 we propose a mechanism for the deformation and alloying process in the nanolaminate. Previous work showed that the yield stress of nanocrystalline Cu (grain size 10 nm, > 3000 MPa) is above that of amorphous
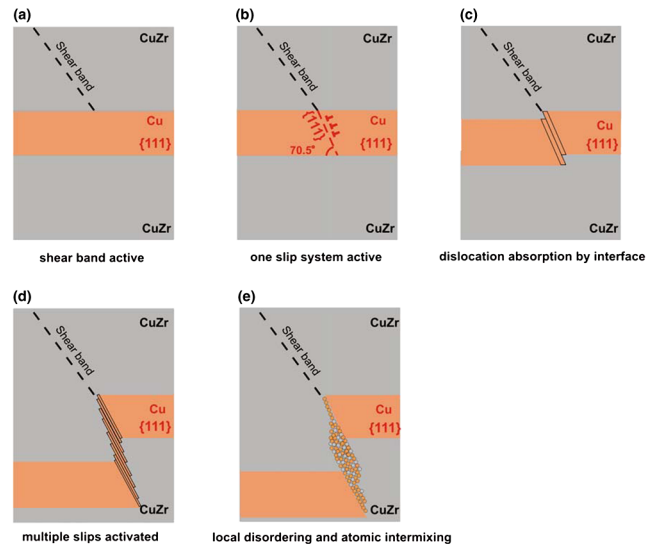

FIG. 4 (color online). Schematic illustration of the proposed mechanism explaining mechanical alloying induced by the crossing of the CuZr/Cu interface by shear dislocations: Nanolaminate deformation proceeds by dislocation slip in the crystalline Cu that coincides with shear bands in the amorphous CuZr layers. Cu atoms are dragged from the crystalline layers across the heterointerfaces when dislocations release their shear into the CuZr phase. Also, complete crystalline Cu nanoclusters are displaced into the amorphous CuZr phase. Both effects lead to massive chemical intermixing between the layers in the 2–3 nm narrow shear band regions.

CuZr(∼2500 MPa).[30] Thus, it is plausible that plastic deformation of the nanolaminate starts by initiating shear transformation zones [31] inside the amorphous CuZr layers and developing them into shear bands, Fig. 4(a) [9–11]. This leads to stress localization when the band impinges the crystalline Cu, activating dislocation nucleation at the amorphous-crystalline interface. The Cu dislocations glide on {111} planes, Fig. 4(b). These dislocations, when crossing from the Cu layer into the amorphous CuZr layer [32], cause a displacement that is an integer multiple of the Cu Burgers vector, Fig. 4(c). The density of mobile dislocations carrying the shear band through the crystalline Cu layer can be calculated by $\rho = \gamma/bl$, where $\gamma = 4.03 \pm 0.18$ is the local offset shear strain, $b = 0.255$ nm is the Burgers vector of Cu, and $l = 10$ nm$/ \sin 70.5° = 10.64$ nm is the mean path of dislocations gliding through the Cu layer into the CuZr/Cu interface.

This estimate gives a mobile dislocation density of ∼1.48×10^{18} m^{-2} inside the Cu shear zone which is 2–3 orders of magnitude above that in heavily deformed Cu [33]. However, this value does not reflect a stored dislocation density. These dislocations are formed at one CuZr/Cu heterointerface and are absorbed at the opposite one, Fig. 4(d). Similar observations on the propagation of shear bands across heterointerfaces in a Zr-Ti-Cu-based

crystal-metallic glass composite were made by Pekarskaya *et al.* [32].

In cases where crystalline portions from the Cu are displaced into the amorphous layer [Fig. 3(b)], very high dislocation densities are found, Figs. 3(c) and 3(d). This observation supports the view of complete crystalline portions being sheared out of the Cu since crystallization due to Cu enrichment would lead to undistorted crystals.

In conclusion, we observe codeformation by shear-dislocation shuffling in crystalline (Cu)–amorphous (CuZr) nanolaminates at scales down to the atomic scale. The mechanism can explain codeformation and shear-induced mixing phenomena in the present context. The mechanism is characterized as follows. (i) Local thinning of the Cu phase can be attributed to the high density of gliding dislocations. (ii) Cu atoms are dragged across the hetero-interface when dislocations release their shear step into the amorphous CuZr phase [Fig. 4(e)]. This leads to intense mixing among the layers inside 2–3 nm narrow shear bands. The Cu enrichment can lead to crystallization. (iii) Besides dislocation driven mixing, nanometer-sized compact portions of crystalline Cu are displaced into the amorphous phase [Figs. 3(b)–3(d)]. This means that the intense chemical intermixing during transphase codeformation includes both individual solute transport via dislocations and collective shear of tiny crystalline portions from the crystalline into the amorphous phase. In the shear banded Cu-enriched zones the initially amorphous CuZr forms an amorphous plus crystalline nanocomposite.

---

*Corresponding author.
guo.w@mpie.de
†Corresponding author.
d.raabe@mpie.de

[1] T. G. Nieh, T. W. Barbee, and J. Wadsworth, Scr. Mater. **41**, 929 (1999).

[2] D. C. Hofmann, J.-Y. Suh, A. Wiest, G. Duan, M.-L. Lind, M. D. Demetriou, and W. L. Johnson, Nature (London) **451**, 1085 (2008).

[3] C. C. Hays, C. P. Kim, and W. L. Johnson, Phys. Rev. Lett. **84**, 2901 (2000).

[4] H. Huang and F. Spaepen, Acta Mater. **48**, 3261 (2000)

[5] T. G. Nieh, J. Wadsworth, C. T. Liu, T. Ohkubo, and Y. Hirotsu, Acta Mater. **49**, 2887 (2001).

[6] J. R. Greer and J. T. M. De Hosson, Prog. Mater. Sci. **56**, 654 (2011).

[7] M. W. Chen, A. Inoue, W. Zhang, and T. Sakurai, Phys. Rev. Lett. **96**, 245502 (2006).

[8] Y. M. Wang, J. Li, A. V. Hamza, and T. W. Barbee, Proc. Natl. Acad. Sci. U.S.A. **104**, 11155 (2007).

[9] C. A. Schuh, T. C. Hufnagel, and U. Ramamurty, Acta Mater. **55**, 4067 (2007).

[10] J.-Y. Kim, D. Jang, and J. R. Greer, Adv. Funct. Mater. **21**, 4550 (2011).

[11] I. Kaban, P. Jovari, V. Kokotin, O. Shuleshova, B. Beuneu, K. Saksl, N. Mattern, J. Eckert, and A. L. Greer, Acta Mater. **61**, 2509 (2013).

[12] T. Gebhardt, D. Music, M. Ekholm, I. A. Abrikosov, J. von Appen, R. Dronskowski, D. Wagner, J. Mayer, and J. M. Schneider, Acta Mater. **59**, 1493 (2011)

[13] P. J. Felfer, T. Alam, S. P. Ringer, and J. M. Cairney, Microsc. Res. Tech. **75**, 484 (2012).

[14] M. Herbig, D. Raabe, Y. J. Li, P. Choi, S. Zaefferer, and S. Goto, Phys. Rev. Lett. **112**, 126103 (2014).

[15] M. J. Duarte, J. Klemm, S. O. Klemm, K. J. J. Mayrhofer, M. Stratmann, S. Borodin, A. H. Romero, M. Madinehei, D. Crespo, J. Serrano, S. S. A. Gerstl, P. P. Choi, D. Raabe, and F. U. Renner, Science **341** (2013) 372.

[16] M. K. Miller and K. F. Russell, Ultramicroscopy **107**, 761 (2007).

[17] K. Thompson, D. Lawrence, D. J. Larson, J. D. Olson, T. F. Kelly, and B. Gorman, Ultramicroscopy **107**, 131 (2007).

[18] J. M. Schneider, B. Hjörvarsson, X. Wang, and L. Hultman, Appl. Phys. Lett. **75**, 3476 (1999).

[19] P. Bas, A. Bostel, B. Deconihout, and D. Blavette, Appl. Surf. Sci. **87**–**88**, 298 (1995).

[20] D. Raabe, P. P. Choi, Y. J. Li, A. Kostka, X. Sauvage, F. Lecouturier, K. Hono, R. Kirchheim, R. Pippan, and D. Embury, MRS Bull. **35**, 982 (2010).

[21] D. Raabe, S. Ohsaki, and K. Hono, Acta Mater. **57**, 5254 (2009).

[22] K. Maier, Phys. Status Solidi A **44**, 567 (1977).

[23] See Supplemental Material at http://link.aps.org/supplemental/10.1103/PhysRevLett.113.035501 for three additional atom probe data sets obtained from the 100 nm CuZr-10 nm Cu multilayer system after 10 g indentation. The strains were quantifying via the offset among neighboring layers. The Cu concentration profiles taken perpendicular through the shear banded are also shown.

[24] X. Quelennec, A. Menand, J. M. Le Breton, R. Pippan, and X. Sauvage, Philos. Mag. **90**, 1179 (2010).

[25] M. Wang, N. Q. Vo, M. Campion, T. D. Nguyen, D. Setman, S. Dillon, P. Bellon, and R. S. Averback, Acta Mater. **66**, 1 (2014).

[26] X. Sauvage, P. Jessner, F. Vurpillot, and R. Pippan, Scr. Mater. **58**, 1125 (2008).

[27] M. Wang, R. S. Averback, P. Bellon, and S. Dillon, Acta Mater. **62**, 276 (2014).

[28] Y. J. Li, P. Choi, C. Borchers, S. Westerkamp, S. Goto, D. Raabe, and R. Kirchheim, Acta Mater. **59**, 3965 (2011).

[29] Y. Z. Chen, A. Herz, Y. J. Li, C. Borchers, P. Choi, D. Raabe, and R. Kirchheim. Acta Mater. **61**, 3172 (2013).

[30] J. Y. Zhang, G. Liu, S. Y. Lei, J. J. Niu, and J. Sun, Acta Mater. **60**, 7183 (2012).

[31] J. S. Langer, Scr. Mater. **54**, 375 (2006).

[32] E. Pekarskaya, C. P. Kim, and W. L. Johnson, J. Mater. Res. **16**, 2513 (2001).

[33] M. R. Staker and D. L. Holt, Acta Metall. **20**, 569 (1972).